

CrossMark  
click for updates

Cite this: DOI: 10.1039/c4tc01997k

# A water-soluble eumelanin polymer with typical polyelectrolyte behaviour by triethyleneglycol N-functionalization†

Stefania R. Cicco,<sup>a</sup> Marianna Ambrico,<sup>b</sup> Paolo F. Ambrico,<sup>b</sup> Maurizio Mastropasqua Talamo,<sup>c</sup> Antonio Cardone,<sup>a</sup> Teresa Ligonzo,<sup>d</sup> Rosa Di Mundo,<sup>e</sup> Cinzia Giannini,<sup>f</sup> Teresa Sibillano,<sup>f</sup> Gianluca M. Farinola,<sup>\*ac</sup> Paola Manini,<sup>g</sup> Alessandra Napolitano,<sup>g</sup> Valeria Criscuolo<sup>g</sup> and Marco d'Ischia<sup>\*g</sup>Received 29th September 2014  
Accepted 14th January 2015

DOI: 10.1039/c4tc01997k

www.rsc.org/MaterialsC

N-functionalization of 5,6-dihydroxyindole with a hydrophilic triethyleneglycol (TEG) chain provides access to a new class of water-soluble eumelanin-like materials with relatively high dielectric constant and polyelectrolyte behaviour, reflecting enhanced charge transport by in-depth incorporation of hydration networks.

## Introduction

Eumelanins, the black insoluble 5,6-dihydroxyindole-based biopolymers responsible for the dark coloration of human skin, hair and eyes,<sup>1</sup> attract growing interest as soft biocompatible and bioavailable multifunctional materials for a broad range of applications, including high-tech hybrid devices, bioelectronics and bionanomedicine.<sup>2,3</sup> Within biological systems, eumelanins are believed to play a variety of roles, *e.g.* photoprotection, antioxidant and metal binding, which depend on a unique combination of physicochemical properties, such as broadband absorption spanning the UV-visible range, efficient non-radiative excited state deactivation, ion storage,<sup>4</sup> a stable free radical character and an unusual water-dependent semiconductor-like behaviour.<sup>5–8</sup>

Since its discovery in the mid 1970's the semiconductor behaviour of eumelanins has raised considerable interest for the design of innovative functional materials for organic

electronics.<sup>9,10</sup> While early theories invoked the amorphous semiconductor model to explain eumelanin electrical properties, more recent evidences suggested an alternative water-dependent ionic–electronic hybrid conductor model. In this model, hydration shifts the comproportionation equilibrium between catechol and *o*-quinone components and semiquinone radicals so as to dope electrons and protons into the system. However, the different hydration dependence of the intrinsic spin density with respect to the electrical conductivity and the  $\mu$ SR relaxation rates suggests a complex interplay of mechanisms that still require elucidation.<sup>7</sup> Eumelanin pigments have also been proposed to serve as biologically derived charge storage materials for application in various types of devices.<sup>4</sup>

Despite the technological potential of eumelanin-based materials and hybrids, several issues related to the insolubility, structural complexity and manifold levels of chemical disorder,<sup>11</sup> account for reported difficulties in the deposition of eumelanin films with controllable thickness,<sup>12</sup> hindering rational property optimization and tailoring for organic electronics applications. Various approaches have been proposed to prepare smooth melanin-based films. DMSO has been shown to be a useful processing solvent, yielding homogeneous and smooth films growing in a quasi-layer-by-layer mode, each layer being composed of nanoaggregates, 1–2 nm high.<sup>13</sup> Good quality synthetic eumelanin (SM) layers were obtained by spin-coating a commercial eumelanin sample onto indium tin oxide (ITO) or silicon surfaces modified by a dry plasma procedure,<sup>14–16</sup> in order to improve adhesion. Investigation of charge carriers and related transport mechanisms across the SM layers led to important insights into the eumelanin-Si/ITO interfaces. By the same procedure, electrically tuneable eumelanin-like polymers from structurally modified polydopamine *via* copolymerization with 3-aminotyrosine and *p*-phenylenediamine were obtained as components of innovative

<sup>a</sup>Istituto di Chimica dei Composti OrganoMetallici ICCOM di Bari, Consiglio Nazionale delle Ricerche CNR, via Orabona 4, 70126-Bari, Italy. E-mail: gianlucamaría.farinola@uniba.it

<sup>b</sup>Istituto per le Metodologie Inorganiche e dei Plasmi IMIP di Bari, Consiglio Nazionale delle Ricerche CNR, via Orabona 4, 70126-Bari, Italy

<sup>c</sup>Dipartimento di Chimica, Università degli Studi di Bari A. Moro, via Orabona 4, 70126-Bari, Italy

<sup>d</sup>Dipartimento di Fisica, Università degli Studi di Bari A. Moro, via Orabona 4, 70126-Bari, Italy

<sup>e</sup>Tribology LAB, Dipartimento di Meccanica, Matematica e Management, Politecnico di Bari, v.le Japigia 182, 70126-Bari, Italy

<sup>f</sup>Istituto di Cristallografia, Consiglio Nazionale delle Ricerche CNR-IC, via Amendola 122/O, 70126-Bari, Italy

<sup>g</sup>Dipartimento di Scienze Chimiche, Università di Napoli "Federico II", Via Cintia 4, 80126-Napoli, Italy. E-mail: dischia@unina.it

† Electronic supplementary information (ESI) available. See DOI: 10.1039/c4tc01997k

metal-insulator-semiconductor (MIS) devices.<sup>17</sup> Very recently, cysteine-containing derivatives of the adhesive biopolymer polydopamine in variable ratios were obtained, showing a marked photoimpedance response to light stimuli.<sup>18</sup> In all these cases, layer deposition was carried out by extensive dissolution of the synthetic pigments in 26% aqueous ammonia.<sup>19</sup> In spite of technological convenience, eumelanin deposition under alkaline conditions would expectedly be accompanied by structural modification due to oxidative degradation.<sup>1</sup> Whether and by what mechanism such structural modifications could affect eumelanin electrical properties is however unclear. A central issue in this context is the possible impact of eumelanin degradation on aggregation and hydration since there are still a number of fundamental gaps concerning the mechanisms by which the aggregation state and water-binding affect the charge transport mechanisms. The supramolecular organization in eumelanin-based materials has been the focus of several studies, and the contribution of orderly  $\pi$ -stacked indolic components has been proposed as being critical for several physicochemical properties.<sup>20,21</sup>

A convenient alternative to dissolution in ammonia for eumelanin thin film processing would be the development of melanin-derivatives soluble in organic solvents by proper functionalization.<sup>22,23</sup> However, achieving water-soluble eumelanins appears more appealing: processing from aqueous media would allow an efficient permeation of water molecules through the bulk of the films and a more efficient charge transport. Furthermore, water is the most suitable biocompatible medium for a biodevice design. Three different and effective methods to obtain largely water-soluble eumelanin-type polymers have been reported. The first method is based on the oxidative polymerization of glycosylated precursors such as 5,6-dihydroxyindole (DHI);<sup>24</sup> the second consists in the oxidation of 5,6-dihydroxyindole substrates in aqueous buffer containing 1% poly(vinyl alcohol) (PVA) to prevent polymer precipitation;<sup>25</sup> the third involves polymerization of suitable precursors in proteins or biological matrix, such as egg white.<sup>26,27</sup> Although these approaches may be useful for the elucidation of eumelanin structural and optical properties, their value for electrical property optimization and semiconductor implementation in devices has still to be assessed and the exploration of novel strategies to improve “solubility-processing approaches” reported in the literature seemed desirable.

Herein we report the synthesis and electrical properties of a new water-soluble eumelanin-like material, triethyleneglycol-melanin (TEGM), obtained by oxidative polymerization of N-functionalized DHI with a hydrophilic TEG group. The underlying rationale is that N-functionalization with TEG chains would favour processability due to water-solubility and would allow for a higher degree of hydration to improve electrical properties.

## Experimental

### General information

All chemicals were purchased from Aldrich, Alfa Aesar and Acros and used without further purification. DMF was distilled

under a reduced pressure over molecular sieves, and stored under nitrogen atmosphere.

FT-IR spectra were measured on a PerkinElmer 1710 spectrophotometer using dry KBr pellets. <sup>1</sup>H and <sup>13</sup>C NMR spectra were recorded in CDCl<sub>3</sub> on a Bruker AM 500 spectrometer at 500 MHz and 125 MHz, respectively.

### Synthesis of 5,6-bis(benzyloxy)-1-(2-(2-(2-methoxyethoxy)ethoxy)ethyl)-1H-indole (2)

NaH (0.078 g, 60% w/w in mineral oil, 1.95 mmol, 1.2 eq.) was introduced in a three-necked round bottom flask under a nitrogen atmosphere. The mineral oil was washed away with hexane, then dry DMF (10 mL) was added. 5,6-Dibenzoyloxyindole (1) (0.536 g, 1.63 mmol, 1 eq.) dissolved in dry DMF (20 mL) was added to the mixture. The resulting mixture was stirred for 30 min, cooled at 0 °C and then 1-bromo-2-(2-(2-methoxyethoxy)ethoxy)ethane (1.541 g, 6.79 mmol, 2.5 eq.) dissolved in dry DMF (10 mL) was added dropwise. The reaction mixture was stirred at room temperature for 4 h, then quenched with saturated aqueous NH<sub>4</sub>Cl, diluted with ethyl acetate and washed many times with water (5 × 20 mL). The organic layer was dried over anhydrous Na<sub>2</sub>SO<sub>4</sub> and the solvent removed under a reduced pressure. The product was purified by silica gel chromatography using a mixture of hexane–ethyl acetate (7 : 3) as the eluent, affording 0.660 g (85% yield) of 2 as a yellowish dense oil.

<sup>1</sup>H NMR (500 MHz, CDCl<sub>3</sub>):  $\delta$  = 7.51–7.50 (m, 4H), 7.39–7.36 (m, 4H), 7.33–7.29 (m, 2H), 7.19 (s, 1H), 7.05 (d, 1H,  $J$  = 3.1 Hz), 6.96 (s, 1H), 6.35 (d, 1H,  $J$  = 3.1 Hz), 5.20 (s, 2H), 5.18 (s, 2H), 4.20 (t, 2H,  $J$  = 5.8 Hz), 3.75 (t, 2H,  $J$  = 5.8 Hz), 3.54 (m, 8H), 3.37 (s, 3H) ppm; <sup>13</sup>C NMR (125 MHz, CDCl<sub>3</sub>):  $\delta$  = 146.57, 144.92, 137.92, 137.65, 131.27, 128.34, 128.31, 127.64, 127.53, 127.46, 127.43, 122.32, 107.16, 100.79, 97.41, 72.46, 72.39, 71.86, 70.70, 70.55, 70.49, 70.10, 58.93, 46.39 ppm; FT-IR:  $\nu$  = 3062, 3030, 2925, 2872, 1505, 1484, 1453, 1420, 1377, 1350, 1302, 1219, 1197, 1142, 1061, 1026, 1004, 914, 876, 849, 760, 740, 697, 648, 597, 470 cm<sup>-1</sup>.

### Synthesis of N-TEG melanin (TEGM)

N-Triethyleneglycol-5,6-dibenzoyloxyindole (2) (0.250 g, 0.53 mmol) in ethyl acetate (30 mL) was poured into a hydrogenation bomb, added with palladium on charcoal (70 mg) and subjected to a positive pressure of hydrogen gas (30 atm). After 18 h the reaction mixture was filtered to remove the catalyst and the solvent evaporated under a reduced pressure. The residue (0.120 g) was taken into methanol (5 mL) and dissolved into an aqueous ammonia solution (1%). The reaction mixture immediately turned into deep violet and after 24 h was dark brown in colour. After 48 h the mixture was acidified to pH 4 with 3 M HCl and evaporated under reduced pressure. The dark residue was taken up in water and freeze-dried overnight to afford TEGM as a dark solid (0.100 g).

### TEGM/SM layers deposition

A TEGM solution for thin film deposition was prepared by dissolving 70 mg of TEGM in deionized water (3 mL). Synthetic

Melanin SM solution for thin film deposition was prepared by dissolving SM powder (70 mg, Sigma-Aldrich) in water (1 mL) and 28% aq ammonia solution (2 mL). The TEGM and SM layers of same thickness were deposited by drop casting on plasma-treated Indium Tin Oxide (ITO)/glass supports. The TEGM and SM layer thickness were measured by an Alpha Step profilometer and both found 400 nm thick (D120, Tencor Instruments). All samples were dried at room temperature under vacuum at a pressure of  $2 \times 10^{-3}$  mbar for 12 h.

### AFM characterization

Surface topography has been characterized by means of an NTEGRA, NT-MDT Atomic Force Microscope in non-contact mode by using high accuracy non-contact (HA-NC) "etalon" probes (high aspect ratio tip, cantilever frequency 140 kHz). Several images at different scan size were acquired on the samples.

### XRD characterization

X-ray diffraction (XRD) analysis of TEGM powders was performed with a Rigaku RINT2500 rotating anode laboratory diffractometer (50 kV, 200 mA) equipped with a silicon strip Rigaku D/teX Ultra detector, using Cu  $K\alpha_1$  monochromatic radiation ( $\lambda = 1.5405$  Å). Moreover, a diffraction pattern has been also acquired from a sample of synthetic melanin (SM) in powder (SIGMA-Aldrich) and on DHI-melanin in powder, in order to compare their structures with that of TEGM (see ESI†).

### MIM device fabrication

A series of metal-insulator-metal (MIM) devices were tailored, for statistical purposes, by thermally evaporating a set of gold (Au) dots ( $\varnothing = 500$   $\mu\text{m}$ , 150 nm thick) on top of the structures consisting of casted TEGM and SM layers.<sup>14,15</sup> A simplified sketch of the typical device configuration and measurement set up adopted in MIM structure characterizations is displayed in Fig. 1.

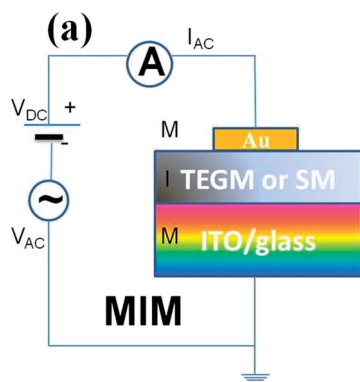


Fig. 1 Scheme of the metal-insulator-metal (MIM) device and of the electrical measurement set up.

### Electrical characterization of TEGM-based MIM devices

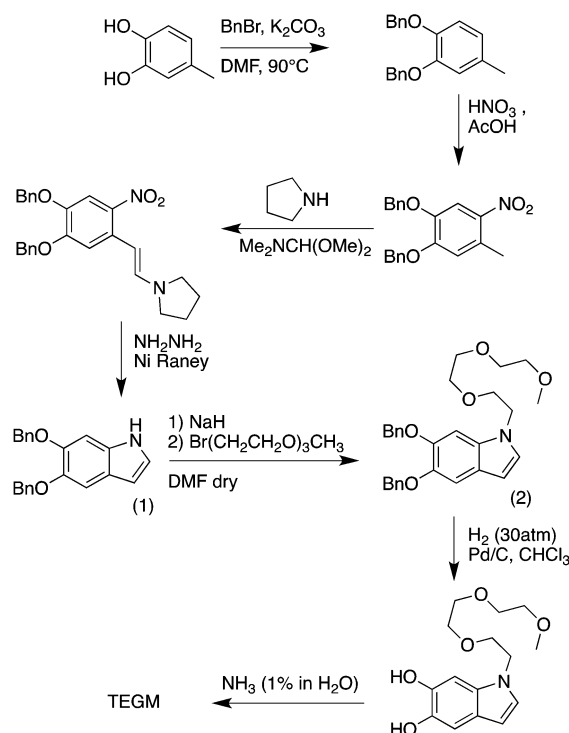
Current–voltage ( $I$  $V$ ) and impedance spectroscopy (IS) measurements have been performed on TEGM-based MIM devices and compared with those collected on SM-based MIM devices. All measurements were performed at room temperature under ambient air at a relative humidity degree of 50%.

Current–voltage hysteresis loops on TEGM-based MIM structures were carried out under dark and by using a Keithley Model 617 electrometer. The loop read outs were performed starting from zero up to a maximum positive value of the continuous bias, defining the hysteresis loop amplitude  $+V_L$ , and then alternating back and forth between  $+V_L$  and  $-V_L$ . The loop amplitudes  $V_L$  were in the range 1.0–3.0 V and the hystereses were acquired at different voltage sweep speeds. Impedance spectroscopy (IS) measurements were made by using a NOVOCONTROL impedance analyzer in the frequency range 0.1 Hz to 1 MHz of the sine wave voltage signal with a signal amplitude  $V_{AC} = 5.0$  mV and at zero DC bias voltage.

## Results and discussion

### TEGM synthesis

TEGM was prepared according to the procedure illustrated in Scheme 1. Briefly, 5,6-dibenzoyloxyindole (1)<sup>28</sup> was N-functionalized with a triethyleneglycol (TEG) chain to give N-TEGylated 5,6-dibenzoyloxyindole (2). Deprotection of 2 by catalytic hydrogenation followed by oxidative polymerization in aqueous ammonia solution led to the formation of a water-soluble



Scheme 1 Synthesis of N-functionalized 5,6-dibenzoyloxyindole (2) and its conversion to TEGM by aerial polymerization after deprotection from benzyl group.

eumelanin-like polymer, which was recovered by evaporation of the aqueous solvent. Black TEGM proved to be freely soluble in water, as verified by filtration on nylon membrane (0.45  $\mu\text{m}$ ). Thin films of TEGM were deposited by drop casting from an aqueous solution onto ITO supports under very mild non-alkaline conditions. UV-vis spectrum of cast TEGM film is reported in the ESI, Fig. S3.†

### TEGM and SM layer characterizations

**AFM and XRD data analyses.** Fig. 2 reports a 10  $\mu\text{m} \times 10 \mu\text{m}$  AFM image of the surface of the TEGM layer deposited on ITO. The surface was fairly smooth except for the presence of micro-scale spaced bumps, not exceeding 90 nm heights. Images acquired at this scan size indicated an average root mean square (RMS) roughness of 7 nm. No other type of structuring could be distinguished at higher resolution scans.

The effect of the TEG chains on eumelanin solid state packing was investigated by X-ray diffraction analysis of TEGM powder in comparison with a commercial synthetic melanin (SM) powder sample as reference. Typically, melanin-like amorphous compounds produce broad peaks in the diffraction spectrum.<sup>23</sup> In the case of TEGM powder, the position of the amorphous peak was found at around  $2\theta \sim 21.5^\circ$ , suggesting a correlation distance  $d = 0.42 \text{ nm}$ , whereas in the case of SM the same peak registered at around  $2\theta \sim 25^\circ$  indicated a distance  $d = 0.35 \text{ nm}$  (Fig. 3), the former being 20% larger compared to the latter.

A correlation distance very similar to that measured for SM was obtained from the XRD spectra of 5,6-dihydroxy-indole-melanin (DHI-Mel). This is a melanin-like material equivalent to TEGM, without the TEG chains, *ad hoc* synthesized for this comparison (Fig. S4, ESI†).

This observation suggests that increased distance is likely due to the presence of the TEG chains on the TEGM polymers.

**Current-voltage and impedance results.** Fig. 4a–c displays the results of current–voltage ( $I$ – $V$ ) hysteresis loops collected in

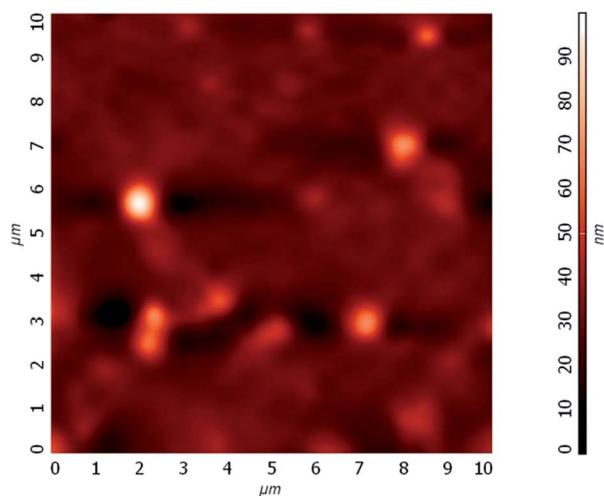


Fig. 2 10  $\mu\text{m} \times 10 \mu\text{m}$  AFM image of the surface of the TEGM layer deposited on ITO.

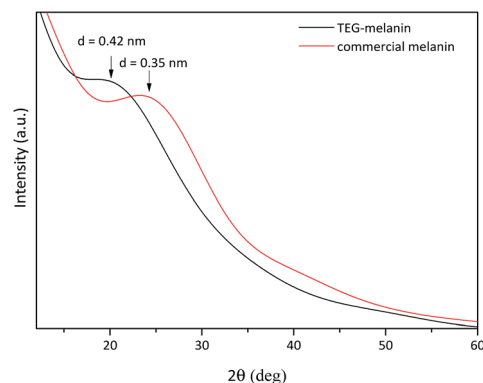


Fig. 3 X-ray diffraction spectra of TEGM (black curve) and commercial melanin SM (red curve).

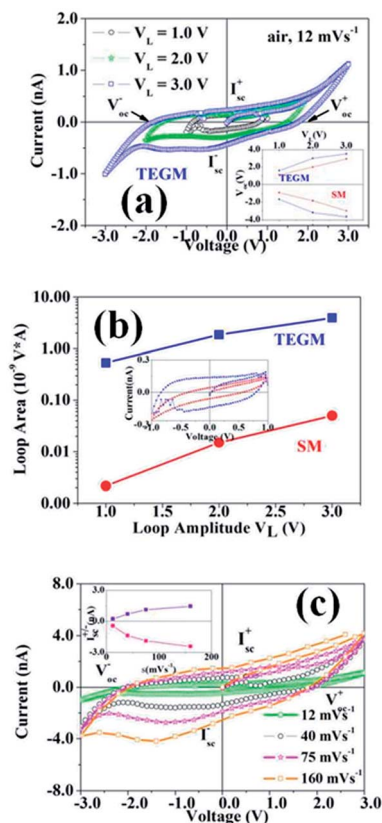


Fig. 4 (a)  $I$ – $V$  hysteresis loops collected on TEGM-based MIM structures at different  $V_L$ . For clarity, the points corresponding to  $V_{oc}^\pm$  and  $I_{sc}^\pm$  have been also indicated. The inset shows the comparison between  $V_{oc}^\pm$  vs.  $V_L$  extracted from TEGM-based and SM-based MIM devices. (b) Loop areas extracted by integrating the  $I$ – $V$  hysteresis loops of SM (red curves) and TEGM (blue curves) at different  $V_L$  values and fixed voltage sweep speed  $s = 12 \text{ mV s}^{-1}$ . The inset shows the comparison between representative loops (at  $V_L = 1 \text{ V}$  and  $s = 12 \text{ mV s}^{-1}$ ) of SM- and TEGM-based MIM devices ( $V_L = 1 \text{ V}$  and  $s = 12 \text{ mV s}^{-1}$ ); (c)  $I$ – $V$  hysteresis loops collected on TEGM-based MIM device at different voltage sweep speeds  $s$  (see legend).  $V_{oc}^\pm$  and  $I_{sc}^\pm$  meanings are the same as in (a). In the inset the extracted values of  $I_{sc}^\pm$  vs.  $s$ .

ambient air on TEGM-based MIM devices for different voltage loop amplitudes,  $V_L$  ( $V_L = 1.0, 2.0$  and  $3.0$  V), while keeping constant the voltage-sweep speed,  $s$ , (a and b) and at different voltage-sweep speeds  $s$  by keeping constant the voltage loop amplitude  $V_L$  (c).

An increase in the voltage loop or in the voltage-sweep speed was found to produce larger hystereses (Fig. 4a–c). Similar results were previously observed in a SM-based MIM structure, confirming that TEGM melanin shows a typical behaviour in space charge storage mechanisms. More specifically, the space charges accumulate at the metal/eumelanin interface, shielding the applied electric field and limiting further carrier injection in the TEGM layer. Based on this hypothesis, the injection occurs during the voltage sweep from 0 V up to  $V_L$  followed by the accumulation at one of the electrodes (Au or ITO); afterwards space charges distribute in the structure. During the reverse sweep and at a certain value of the applied voltage, called open-circuit voltage  $V_{oc}^+$  a balance is established between the external field and that due to space charge so that no current is flowing any longer. By further decreasing the voltage, the current flows again and at zero bias a non-zero current (negative short circuit current,  $I_{sc}^-$ ) is observable due to the stored charges flowing back through the external circuit. Moving toward a more negative voltage (from 0 to  $-V_L$ ), charge storage occurs again and in the subsequent forward sweep direction from ( $-V_L$  up to  $+V_L$ ) an open circuit voltage ( $V_{oc}^-$ ) and a positive short circuit current ( $I_{sc}^+$ ) can be detected. The magnitude of  $I_{sc}^\pm$  and  $V_{oc}^\pm$  in both sweep directions depends on the amount of stored charges at electrode/polymer interface and may differ in the two hysteresis branches due to the different electrode (Au and ITO) work functions.<sup>29</sup>

To detail better on the observed charge storage effect and hysteretic behaviour, we start considering the general expression of the displacement current  $I_d$  as a function of the voltage flowing across a capacitive medium:<sup>29,30</sup>

$$I_d = \frac{dQ}{dt} = \frac{d(CV)}{dt} = V \frac{dC}{dt} + C \frac{dV}{dt} = V \frac{dC}{dt} + Cs \quad (1)$$

Such a current adds to conduction current component  $I_r$ . It can be deduced that the displacement current can be more or less enhanced depending on the voltage loop amplitudes and on the voltage sweep speeds. The term  $(dC/dt)$  represents the increase of capacitance during the voltage sweep.

When fixing the voltage sweep speed  $s$ , (see Fig. 4a) the variation of the amount of stored charges vs.  $V_L$ , can be obtained by integrating expr. (1) *i.e.* by calculating the loop area values (see Fig. 4b). The results indicate that the stored charges are almost linearly dependent on the magnitude of the voltage loop amplitude. The comparison between results on TEGM-based and SM-based MIM devices evidences that in the former the stored charge is two order of magnitude higher than in the latter, thus indicating a more effective space charge accumulation mechanisms under a voltage stimulus. This is also evidenced by the comparison between two typical hysteresis loops collected at the same voltage sweep speed  $s$  and for  $V_L = 1.0$  V on

TEGM-based (blue squares) and on SM-based (red squares) MIM devices (see inset in Fig. 4b).

Furthermore, the hysteresis curves showed an increase of the loop area with voltage sweep speed  $s$  at a fixed voltage loop. Interestingly, in this case the open circuit voltage values kept approximately the same values, while the short circuit currents increased with speed in both hysteresis branches. Based on the expression (A) the zero bias short circuit current  $I_{sc}$  when varying the voltage sweep speed by keeping constant the voltage loop magnitude, could be ascribed to the dependence of the charge-trapping/detrapping mechanisms on the voltage sweep rate. In this case:

$$I_{sc} \sim C \left( \frac{dV}{dt} \right) = Cs \quad (2)$$

*i.e.* a linear dependence of  $I_{sc}$  on  $s$  would be expected. The  $I_{sc}^\pm$  vs.  $s$  data displayed in the inset of Fig. 4c suggested that two linear regimes were present, one at lower voltage sweep speed (up to  $s \leq 60$   $\text{mV s}^{-1}$ ) the other up to  $s = 160$   $\text{mV s}^{-1}$ . By linearly fitting  $I_{sc}^+$  vs.  $s$  values the capacitance varied from 14 nF down to 4 nF as resulting for the low (*i.e.*  $s \leq 60$   $\text{mV s}^{-1}$ ) and high  $s$  values range, respectively. A similar capacitance reduction (*i.e.* from 22 nF to 6 nF going from the low to the high  $s$  values range) was observed by linearly fitting  $I_{sc}^-$  vs.  $s$  values. This variation was ascribed to the distribution and density of charge trapping sites contributing to the capacitance depending on the specific trapping/detrapping characteristic times. The estimate of the SM capacitance resulting from the data collected on SM-based MIM devices indicated that the layer capacitance was lower than that of the TEGM layer (55 pF for the low  $s$  range *i.e.*  $s = 1.0$ – $12$   $\text{mV s}^{-1}$ ).

**Impedance measurements results.** The electrical transport properties of both TEGM and SM appeared to depend on the water-ion content, so that they can both be assigned to the class of water-based polyelectrolytes.<sup>31</sup> The analysis of the AC impedance frequency dispersion can provide further insight into the relative extent of the different relaxation mechanisms contributing to the spectra as a result of electrode polarization, ionic motion and possible dipolar contributions.

Fig. 5 illustrates the real ( $\epsilon'$ , dielectric constant) and imaginary ( $\epsilon''$ , dielectric loss) part of dielectric permittivity frequency dispersion, as derived from the impedance data collected in ambient air on TEGM- and SM-based MIM structures. In the inset the loss factor  $\tan \delta$  vs.  $f$  dispersion, *i.e.* the ratio between the dielectric loss and dielectric constant, is also shown. Interestingly, different behaviours of TEGM and SM permittivity were observed.

The real part of the dielectric permittivity spectra of TEGM revealed the presence of a plateau in the frequency region up to 10 Hz, assigned to the double layer capacitive contribution. Relevant to note, the estimated dielectric constant is two orders of magnitude higher than that of SM, evidencing an increased interfacial polarization effect at the electrode. In the frequency region 10 Hz to 10 kHz the TEGM dielectric constant shows a behaviour typically observed in polyelectrolytes and its value was consistently higher than that of SM. This can be attributed to the recognized ability of TEG to increase ionic conductivity

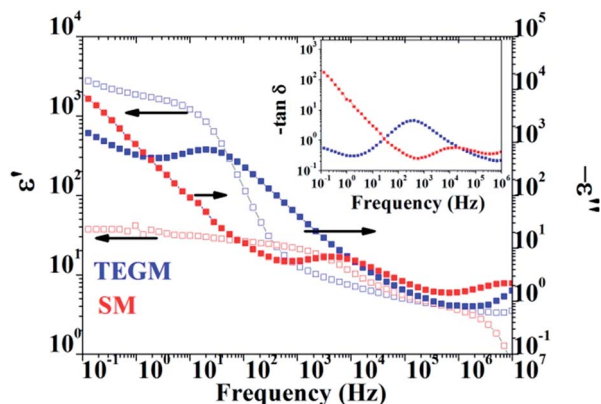


Fig. 5 Dispersion spectra of the real ( $\epsilon'$ , left axis) and imaginary ( $\epsilon''$ , right axis) part of the dielectric permittivity as resulting from impedance spectra collected on TEGM (blue curves) and SM (red curves) MIM devices. The inset shows the calculated  $\tan \delta$  loss dispersion spectra.

and/or dipolar effects, as observed in other polymers. Furthermore, a major water molecules enclosure should be expected due to the TEG major hydrophilicity.<sup>32</sup> The relaxation process then extends up to 1 MHz and the corresponding relaxation time was extracted by the peak frequency in the loss  $\tan \delta$  vs.  $f$  spectra and found to be  $\tau = 2.56$  ms.<sup>32</sup>

Compared to TEGM, the  $\epsilon'$  of SM showed a dispersion spectrum whose behaviour was similar to those commonly observed in biological items. In particular, the two typical regions generally encountered in biological items  $\epsilon'$  spectra, were distinguishable. The first one was constituted by a relaxation region generally extending from 1 kHz up to 1 MHz and whose magnitude is strictly related to the embedded water content. Such a region is commonly referred to as the  $\beta$  region (see ESI†). The second one, at a relaxation frequency above 1 MHz, evidenced the presence of the water-molecule dipole reorientation processes and was commonly defined as the  $\gamma$ -region (see ESI†).<sup>33</sup>

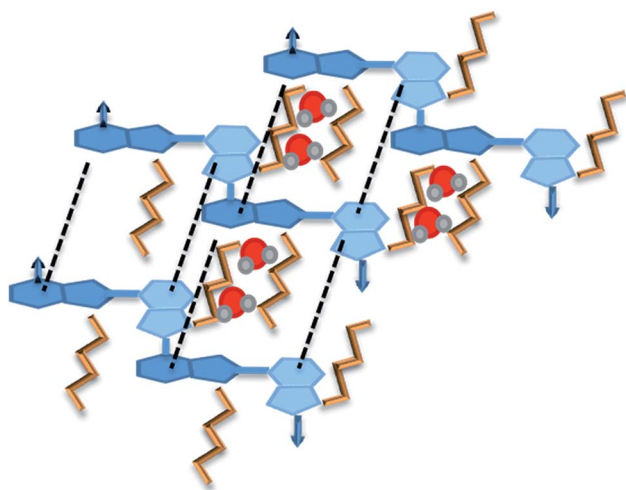


Fig. 6 Pictorial model of possible assembly of TEGM with water incorporation.

Data in Fig. 4 and 5 clearly showed that the inclusion of the highly hydrophilic TEG chain results in a profound alteration of typical eumelanin electrical properties with a marked increase in the dielectric constant and a distinct polyelectrolyte behaviour. It is suggested that the TEG chains allow for the incorporation of water molecules into the bulk of the eumelanin films, with the formation of a hydrogen-bond network enabling efficient charge transport in the solid state. It is tempting to assume, in this context, that the oligoether chains play the dual role of favouring eumelanin aggregation in a relatively regular manner and keeping the water molecules tightly bound between the stacked indolic layers (Fig. 6).

## Conclusions

A water soluble eumelanin biopolymer TEGM is described, which was obtained by oxidative polymerization of a DHI derivative N-substituted with a hydrophilic TEG chain. Current-voltage measurements in MIM devices indicated markedly higher open circuit values and hysteresis loop areas in the case of TEGM compared to the commercial melanin SM, suggesting in the former a more effective space charge mechanism. Impedance data consistently indicated for TEGM a double layer contribution much higher than for the reference SM and a higher dielectric constant. These results point to DHI functionalization with the solubilizing and highly hydrophilic TEG chain as an effective approach to confer polyelectrolyte behaviour to eumelanin materials, possibly *via* the formation of a hydration shell around oligomer molecular components.

## Acknowledgements

Prof. Giuseppe Carbone is gratefully acknowledged for allowing to use the Atomic Force Microscope of the Tribology Lab (DMMM, Politecnico di Bari). This work was supported in part by grants from MIUR, PRIN 2010–2011 (PROxi project) and 2012 (AQUASOL Project PRIN2012 A4Z2RY), by the FIRB 2009/2010 project “Rete integrata per la Nano Medicina (RINAME)” – RBAP114AMK\_006 and in part by European Commission (PolyMed project in the FP7-PEOPLE-2013-IRSES frame, r.n.PIRSES-GA-2013-612538) and was carried out in the frame of the activities of the EuMelaNet special interest group. Giuseppe Chita is acknowledged for technical support in the RINT2500 laboratory.

## Notes and references

- 1 M. d'Ischia, K. Wakamatsu, A. Napolitano, S. Briganti, J.-C. Garcia-Borron, D. Kovacs, P. Meredith, A. Pezzella, M. Picardo, T. Sarna, J. D. Simon and S. Ito, *Pigm. Cell Melanoma Res.*, 2013, **26**, 616–633.
- 2 M. d'Ischia, A. Napolitano, V. Ball, C. Chen and M. J. Buehler, *Acc. Chem. Res.*, 2014, **47**, 3541–3550.
- 3 P. Meredith, C. J. Bettinger, M. Irimia-Vladu, a B. Mostert and P. E. Schwenn, *Rep. Prog. Phys.*, 2013, **76**, 034501.
- 4 Y. J. Kim, W. Wu, S. Chun, J. F. Whitacre and C. J. Bettinger, *Proc. Natl. Acad. Sci. U. S. A.*, 2013, **110**, 20912–20917.

- 5 M. Rozanowska, T. Sarna, E. J. Land and T. G. Truscott, *Free Radical Biol. Med.*, 1999, **26**, 518–525.
- 6 A. B. Mostert, B. J. Powell, I. R. Gentle and P. Meredith, *Appl. Phys. Lett.*, 2012, **100**, 093701.
- 7 A. B. Mostert, B. J. Powell, F. L. Pratt, G. R. Hanson, T. Sarna, I. R. Gentle and P. Meredith, *Proc. Natl. Acad. Sci. U. S. A.*, 2012, **1–5**.
- 8 P. Meredith and T. Sarna, *Pigm. Cell Res.*, 2006, **19**, 572–594.
- 9 J. McGinness, P. Corry and P. Proctor, *Science*, 1974, **183**, 853–855.
- 10 G. Mula, L. Manca, S. Setzu and A. Pezzella, *Nanoscale Res. Lett.*, 2012, **7**, 377.
- 11 N. F. Della Vecchia, R. Avolio, M. Alfè, M. E. Errico, A. Napolitano and M. d'Ischia, *Adv. Funct. Mater.*, 2013, **23**, 1331–1340.
- 12 F. Bernsmann, V. Ball, F. Addiego, A. Ponche, M. Michel, J. J. D. A. Gracio, V. Toniazzi and D. Ruch, *Langmuir*, 2011, **27**, 2819–2825.
- 13 J. Wünsche, F. Cicoira, C. F. O. Graeff and C. Santato, *J. Mater. Chem. B*, 2013, **1**, 3836.
- 14 M. Ambrico, P. F. Ambrico, A. Cardone, T. Ligonzo, S. R. Cicco, R. Di Mundo, V. Augelli and G. M. Farinola, *Adv. Mater.*, 2011, **23**, 3332–3336.
- 15 M. Ambrico, A. Cardone, T. Ligonzo, V. Augelli, P. F. Ambrico, S. Cicco, G. M. Farinola, M. Filannino, G. Perna and V. Capozzi, *Org. Electron.*, 2010, **11**, 1809–1814.
- 16 M. Ambrico, P. F. Ambrico, T. Ligonzo, A. Cardone, S. R. Cicco, A. Lavizzera, V. Augelli and G. M. Farinola, *Appl. Phys. Lett.*, 2012, **100**, 253702.
- 17 M. Ambrico, P. F. Ambrico, A. Cardone, N. F. Della Vecchia, T. Ligonzo, S. R. Cicco, M. M. Talamo, A. Napolitano, V. Augelli, G. M. Farinola and M. d'Ischia, *J. Mater. Chem. C*, 2013, **1**, 1018.
- 18 M. Ambrico, N. F. Della Vecchia, P. F. Ambrico, A. Cardone, S. R. Cicco, T. Ligonzo, R. Avolio, A. Napolitano and M. d'Ischia, *Adv. Funct. Mater.*, 2014, **24**, 7161–7172.
- 19 J. P. Bothma, J. de Boor, U. Divakar, P. E. Schwenn and P. Meredith, *Adv. Mater.*, 2008, **20**, 3539–3542.
- 20 A. A. R. Watt, J. P. Bothma and P. Meredith, *Soft Matter*, 2009, **5**, 3754.
- 21 C.-T. Chen, C. Chuang, J. Cao, V. Ball, D. Ruch and M. J. Buehler, *Nat. Commun.*, 2014, **5**, 3859.
- 22 K. J. Lawrie, P. Meredith and R. P. McGeary, *Photochem. Photobiol.*, 2008, **84**, 632–638.
- 23 S. N. Dezidério, C. A. Brunello, M. I. N. da Silva, M. A. Cotta and C. F. O. Graeff, *J. Non-Cryst. Solids*, 2004, **338–340**, 634–638.
- 24 A. Pezzella, A. Iadonisi, S. Valerio, L. Panzella, A. Napolitano, M. Adinolfi and M. d'Ischia, *J. Am. Chem. Soc.*, 2009, **131**, 15270–15275.
- 25 A. Pezzella, V. Ambrogio, M. Arzillo, A. Napolitano, C. Carfagna and M. d'Ischia, *Photochem. Photobiol.*, 2010, **86**, 533–537.
- 26 A. Chassepot and V. Ball, *J. Colloid Interface Sci.*, 2014, **414**, 97–102.
- 27 N. F. Della Vecchia, P. Cerruti, G. Gentile, M. E. Errico, V. Ambrogio, G. D'Errico, S. Longobardi, A. Napolitano, L. Paduano, C. Carfagna and M. d'Ischia, *Biomacromolecules*, 2014, **15**, 3811–3816.
- 28 D. Batcho and W. Leimgruber, *Org. Synth.*, 1985, **63**, 214.
- 29 H. S. Majumdar, A. Bandyopadhyay, A. Bolognesi and A. J. Pal, *J. Appl. Phys.*, 2002, **91**, 2433.
- 30 H. S. Majumdar, A. Bandyopadhyay, A. Bolognesi and A. J. Pal, *J. Appl. Phys.*, 2002, **91**, 5508.
- 31 G. Schwarz, *J. Phys. Chem.*, 1962, **66**, 2636–2642.
- 32 D. K. Pradhan, R. N. P. Choudhary and B. K. Samantaray, *Int. J. Electrochem. Sci.*, 2008, **3**, 597–608.
- 33 H. P. Schwan, in *Advances in Biological and Medical Physics*, ed. J. H. Lawrence and C. A. Tobias, Academic Press Inc., New York, 1957, vol. 5, pp. 147–209.